

Supporting Information for “Hydrosilylation of carbonyls over electron-enriched Ni sites of intermetallic compound Ni₃Ga heterogeneous catalyst”

Tomoaki Takayama,^a Rio Kariya,^a Yuki Nakaya,^b Shinya Furukawa,^{b, c, d*} Seiji Yamazoe,^{c, d, e}
Takayuki Komatsu^{a*}

^aDepartment of Chemistry, School of Science, Tokyo Institute of Technology, 2-12-1-E1-10 Ookayama, Meguro-ku, Tokyo 152-8551, Japan.

^bInstitute for Catalysis, Hokkaido University, N21, W10, Kita-ku, Sapporo 001-0021, Japan.

^cElements Strategy Initiative for Catalysts & Batteries (ESICB), Kyoto University, 1-30 Goryo-Ohara, Nishikyo-ku, Kyoto 615-8245, Japan.

^dJapan Science and Technology Agency, PRESTO, Chiyodaku, Tokyo, Japan, 102-0076

^eDepartment of Chemistry, Graduate School of Science, Tokyo Metropolitan University, 1-1 minami-Osawa, Hachioji-shi, Tokyo 192-0397, Japan.

Experimental details

Catalyst preparation

The supported Ni-based bimetallic catalysts (Ni loading, 5 wt% of weight of a SiO₂ support; Ni_xM_y/SiO₂, M = Ga, Ge, or In; Ni-M'/SiO₂, M' = Cu, Co, or Fe, atomic ratio of Ni/M' = 1) were prepared by co-impregnation combined with the pore-filling protocol. SiO₂ (CARiACT G-6, Fuji Silysia Chemical) was dried in an automatic oven (120°C) and then employed as the support. Starting materials for the intermetallic compounds are summarized as follows; Ni(NO₃)₂·6H₂O (Soekawa Chemical; 99.9%), Ga(NO₃)₃·*n*H₂O (*n* = 7–9, FUJIFILM Wako Pure Chemical; 99.9%), (NH₄)₂GeF₆ (Sigma Aldrich; 99.99%), In(NO₃)₃·*n*H₂O (Kanto Chemical; 99.9%), Cu(NO₃)₂·3H₂O (Kanto Chemical; 77~80% as Cu(NO₃)₂), Co(NO₃)₂·6H₂O (Kanto Chemical; 98%), Fe(NO₃)₃·9H₂O (Wako Pure Chemical; 99%). A specific volume of an aqueous solution containing both nickel and second metal salts was added dropwise to the dry SiO₂ powder. For the intermetallic compounds, atomic ratios of Ni to second metal (denoted as M or M' above) were equivalent to their compositional formula; e.g., Ni₃Ga, atomic ratio of Ni/Ga = 3. After the obtained slurry was stirred by a glass rod, it was covered with a plastic film and sequentially kept mixed at room temperature overnight. After that, the slurry was completely dried on a hot plate (120°C) to obtain the powdered sample. The powder was reduced in a quartz tube (inner diameter: 12 mm) under hydrogen flow (60 mL min⁻¹) at 800°C for 1 h in order to obtain particulate intermetallic compounds supported on SiO₂. For Ni₃Ga/SiO₂, ethanol was also employed as the solution containing the metal salts instead of water. The obtained slurry was dried under reduced pressure using an evaporator equipped with a water bath at 70°C after drying on a hot plate (70°C), followed by the same reduction manner as the preceding procedure, which was the optimum condition at the present stage. As-impregnated Ni-Ga/SiO₂ was prepared by the same manner as the optimum condition without hydrogen reduction at 800°C for 1 h and used for H₂-TPR analysis shown in Figure S8. Ga/SiO₂ was prepared by the same manner as the optimum condition using Ga(NO₃)₃·*n*H₂O (*n* = 7–9) as the metal source and used as the reference sample for the hydrosilylation reaction shown in Figure S4.

Characterization of the catalysts

The crystal phases of the catalysts were identified by powder X-ray diffraction (XRD) using a Cu K α X-ray source with the tube voltage of 40 kV and the tube current of 40 mA (BRUKER; D8 Advance). The scan was performed over the range (2θ) from 30° to 60° in the scan step of 0.01° with the scan speed of 0.3°/min. To evaluate the reduction behavior of the catalyst, temperature-programmed reduction (TPR) was performed. Prior to the TPR measurement, the catalyst powder (50 mg) was heated at 200°C for 0.5 h to remove the adsorbed water under an Ar stream (30 mL min⁻¹). The temperature of the sample bed was then raised from room temperature to 900°C at a heating rate of 10°C min⁻¹ under a H₂(5%)/Ar stream. The consumption of hydrogen was continuously measured by an online gas-chromatograph equipped with a thermal conductivity detector. Inductively coupled plasma optical emission spectrometer (ICP-OES; Shimadzu ICPE-9000 spectrometer) analysis was

conducted to detect the leached metals from the catalysts. After filtration of the spent catalyst and zeolite dispersed in the reaction solution using a glass syringe equipped with a membrane filter (DISMIC-13JP, Toyo Roshi Kaisha, Ltd.; pore size: 0.2 μm), the filtrate (2 mL) was gradually dried up in a glass vial on a hot plate (60°C). After the filtrate was completely dried up, nitrohydrochloric acid (15 mL) was added into the vial and retained at 60°C for 10 min. The acid solution was diluted in a measuring flask (25 mL) with deionized water to obtain the sample for the ICP-OES analysis. CO-pulse chemisorption was performed using BELCAT II (Microtrac BEL) to estimate the Ni dispersion of the supported intermetallic compound catalysts. The catalyst was reduced under a H₂(5%)/Ar flow (40 mL min⁻¹) at 400°C for 0.5 h. After the reduction treatment, He gas was introduced at the same temperature for 10 min to remove the chemisorbed hydrogen, followed by cooling to room temperature. A CO(10%)/He pulse was introduced into the sample cell at -100°C, and the residual CO in the flow gas was quantified downstream by a thermal conductivity detector. The number of Ni atoms of the catalyst surface was defined as equal to that of the chemisorbed CO molecules. The X-ray absorption fine structure (XAFS) spectra at Ni K-edge (8.3 keV) and Ga K-edge (10.4 keV) were measured at the BL01B1 beamline of the SPring-8 facility with the ring energy of 8 GeV and a stored current from 60 to 100 mA. The XAFS spectra were obtained by transmittance mode with quick scan at room temperature using Si(111) double-crystal monochromators. Prior to the measurements, the SiO₂-supported Ni-based intermetallic compounds were elaborately grinded using an agate mortar and then pelletized, followed by reduction under a H₂ gas at 400°C for 1 h. As the reference sample, a Ni₃Ga/SiO₂ pellet without the reduction at 400°C was prepared (denoted as as-prepared Ni₃Ga/SiO₂). After that, the pellets were separately sealed into a polyethylene bag with an oxygen absorber (I. O. S. Inc.; A-500HS) under a dry N₂ gas without exposure to the air. NiO and Ga₂O₃ powders and fragments of bulk Ga were elaborately mixed with BN (boron nitride) using an agate mortar and pelletized without any pretreatment. The X-ray absorption near edge structure (XANES) and extended X-ray absorption fine structure (EXAFS) analyses were conducted by the Athena software.¹ For the Ni K-edge EXAFS analyses, the absorption main edges of the XAFS spectra were fixed at the center between those of a Ni foil and the NiO pellet. As for the Ga K-edge EXAFS analyses, those absorption edges were fixed by the same manner to the preceding one using the Ga pellet and the Ga₂O₃ pellet. The EXAFS oscillations ranged from 3.0 to 15.0 of the k range (\AA^{-1}) were Fourier transformed.

Evaluation of catalytic performances for hydrosilylation

The reaction apparatus was constructed by a 50 mL three-neck round-bottom flask equipped with a silicone rubber septum, a reflux condenser, and a gas storage balloon (2 L). A catalyst (250 mg) was placed in the flask with zeolite (250 mg; synthetic A-3 powder, Wako Pure Chemical Industries) that was employed as a dehydrating reagent. The pre-treatment of the catalyst was conducted under a H₂ stream at 400°C for 1 h using a mantle heater. After the pre-treatment, the flask was purged with dry Ar to replace the residual H₂ and then cooled to room temperature. The gas storage balloon was filled with the dry Ar gas. Tetrahydrofuran (THF; >99.5%, Kanto Chemical, Supper dehydrated) of the

solvent (5 mL; an Ar balloon should be equipped with the bottle during the extraction of the THF solution using a glass syringe), triethylsilane (0.2 mmol; >98.0%, Tokyo Chemical Industry) and 2-cyclohexen-1-one (0.1 mmol; >96.0%, Tokyo Chemical Industry) of the reactants, and dodecane of the internal standard (0.1 mmol; FUJIFILM Wako Pure Chemical) was mixed and immediately added to the flask through the septum. Other reagents were used so as to evaluate the scope of hydrosilylation and are summarized as follows; cyclohexanone (>99%; Wako Pure Chemical), acetone (>99.0%; Kanto Chemical), 2-pentanone (>99.0%; Tokyo Chemical Industry), 3-pentanone (>98.0%; Tokyo Chemical Industry), 2,4-dimethyl-3-pentanone (>98.0%; Tokyo Chemical Industry), acetophenone (98.5%; Tokyo Chemical Industry), pentanal (>95.0%; valeraldehyde, Tokyo Chemical Industry), hexanal (>98.0%; Tokyo Chemical Industry), benzaldehyde (>99.5%; Sigma-Aldrich), 4-(trifluoromethyl)benzaldehyde (>95.0%; Tokyo Chemical Industry), *p*-anisaldehyde (99.0%; Tokyo Chemical Industry), dimethylphenylsilane (>97.0%; Tokyo Chemical Industry), triphenylsilane (>96.0%; Tokyo Chemical Industry). The catalytic reaction was initiated by the addition of the mixture into the reaction apparatus at room temperature or 70°C using an oil bath. The products were quantified by a gas chromatograph with a flame ionization detector (FID) (Shimadzu GC-18B equipped with a capillary column, TC-70 GL Science or SH-Rtx-1701 Shimadzu GLC) and GC-MS (Shimadzu GCMS-QP2010 SE; SH-Rtx-1701 capillary column). The conversions of 2-cyclohexen-1-one and other ketone and aldehyde substrates, and the yields of the corresponding silyl enol ethers or silyl ethers were defined as shown in the following equations;

$$\text{Conversion (\%)} = \left(1 - \frac{N_{\text{residual substrate}}}{N_{\text{initial substrate}}}\right) \times 100 \quad (1)$$

$$\text{Yield (\%)} = \left(\frac{N_{\text{product}}}{N_{\text{initial substrate}}}\right) \times 100 \quad (2)$$

where, *N* indicates the relative number of the substrate molecule, which is the ratio of the standardized GC peak area of the substrate to that of dodecane of the internal standard. The standardized GC peak area was estimated by dividing the raw GC peak area of the substrate by the corresponding GC factor (*e.g.*, for the GC factor, aliphatic carbon atom: 1.00, olefinic carbon atom: 0.95, carbonyl: 0.00, -CH-OSi(C₂H₅)₃: 6.69, aromatic carbon atom: 1.00, fluorine atom on aliphatic carbon: -0.12 (this value was defined to be the same as that of chlorine atom on aliphatic carbon atom), oxygen atom of ether: -1.00. The raw GC peak area was estimated using the gas-chromatograph equipped with FID. *N*_{initial substrate} was estimated by the initial concentration of the substrate in the hydrosilylation reaction. *N*_{residual substrate} or *N*_{product} was estimated by the concentration of the substrate or that of the obtained silyl enol ether, silyl ether, or by-product in the hydrosilylation reaction at the predetermined time.

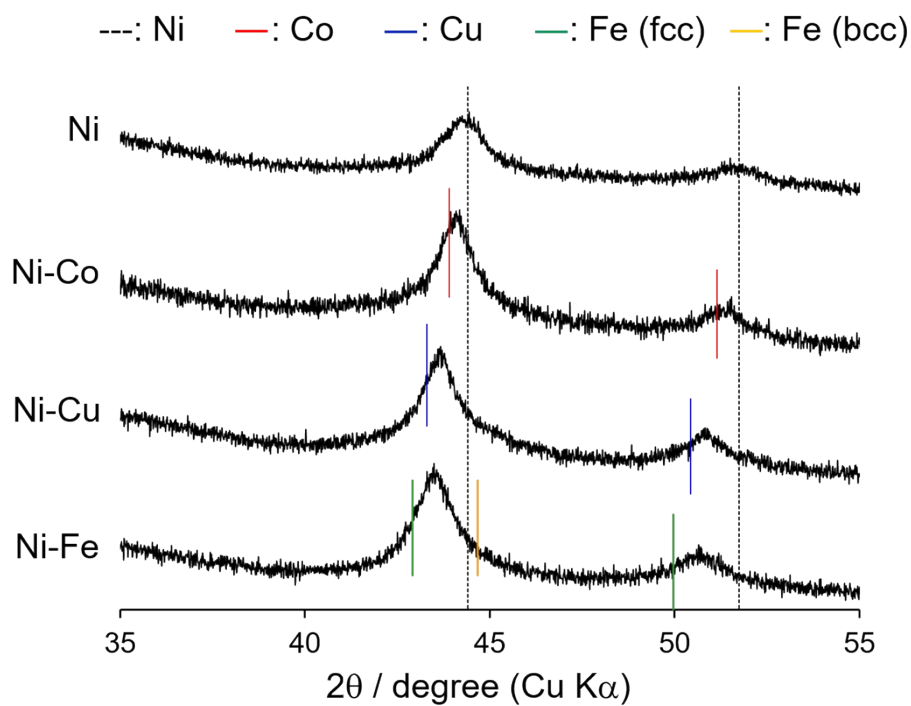


Figure S1. XRD patterns of Ni-based solid-solution alloys supported on SiO₂. The dashed and solid lines indicate diffraction peak positions of Ni and each of the second metals, which are listed in the PDFs; Ni: 4-850, Co: 1-71-4238, Cu: 4-836, Fe (fcc): 3-65-4150, Fe (bcc): 6-696.

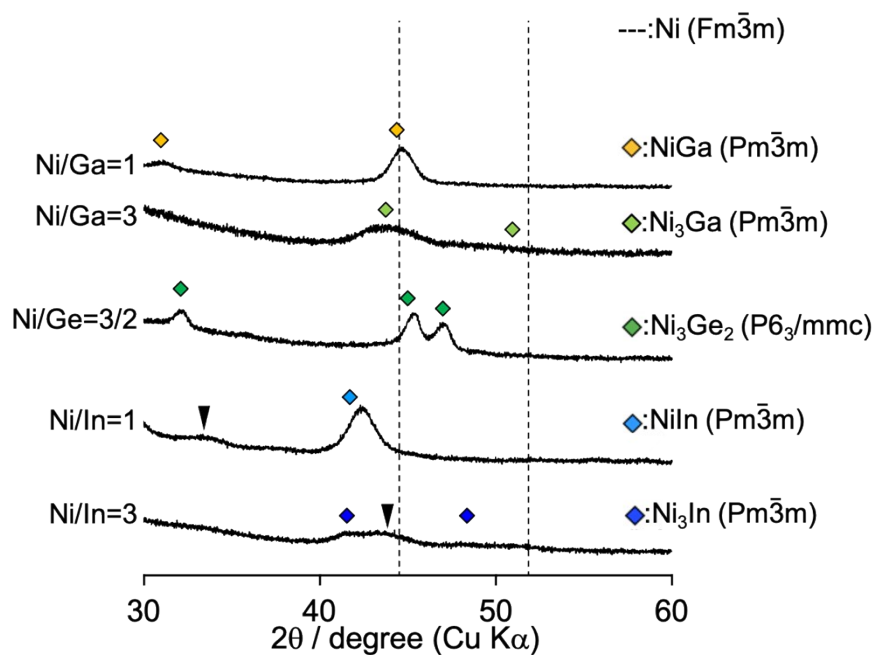


Figure S2. XRD patterns of Ni-based intermetallic compounds supported on SiO₂. The space groups of the intermetallic compounds are displayed in parentheses. The dashed lines and the rhomboidal makers indicate diffraction peak positions of the PDFs; Ni: 4-850, NiGa: 1-71-8616, Ni₃Ga: 1-71-8620, Ni₃Ge₂: 1-89-7599, NiIn: 1-73-8952, Ni₃In: 1-75-6572.

Comment on Figures S1 and S2:

X-ray diffraction patterns of the catalysts were measured to identify those crystal phases. Single phase Ni was loaded on the silica support, judging from agreement of the observed peak position with the reference position (Figure S1). For the alloy catalysts prepared by the atomic ratio of Ni/M = 1 (M = Co, Cu, or Fe), their diffraction peaks were located at the almost center position between Ni and either of the second metals except for Fe (bcc). This suggests formation of solid-solution alloys possessing the fcc crystal structure. As for the XRD patterns shown in Figure S2, NiGa, Ni₃Ga, and Ni₃Ge₂ were successfully obtained on the supports without any crystalline impurity phase, judging from the fact that the observed peak positions were almost consistent with the reference positions. NiIn and Ni₃In were certainly formed on SiO₂ accompanied by formation of unknown phases displayed as inverted closed triangles.

Table S1. Hydrosilylation over the Ni₃Ga/SiO₂ catalyst with/without zeolite.

Entry	Zeolite	Time / h	Conv. (%)	Yield (%)	
				Silyl enol ether	cyclohexanone
1	Yes	6	95	69	20
2	No	3	100	50	30

Catalyst: 250 mg, zeolite (synthetic A-3 powder): 250 mg, THF: 5 mL, triethylsilane: 0.2 mmol, 2-cyclohexen-1-one: 0.1 mmol, dodecane: 0.1 mmol, under Ar (1 bar), room temperature. Ni₃Ga was prepared by the optimized procedure. Ni: 4 mol%; *i.e.*, the number of surface Ni atoms of Ni₃Ga/SiO₂ (250 mg, Ni: 5 wt%) is 4% of the mole of 1-cyclohexen-1-one of the substrate, which is explained in the comment on Figure S11.

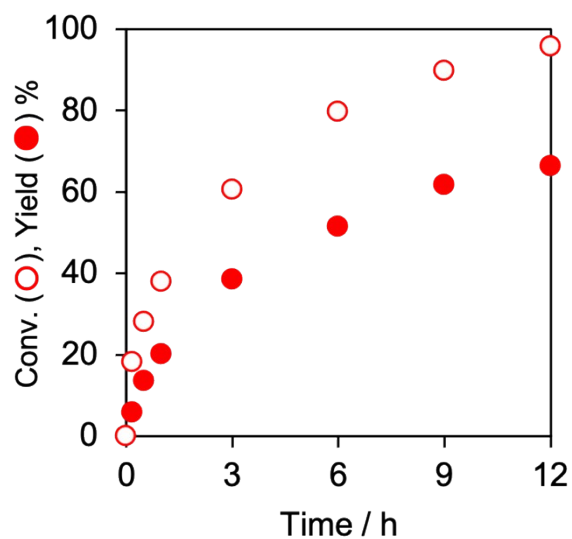


Figure S3. Time course of the hydrosilylation of 2-cyclohexen-1-one over the Ni₃Ga/SiO₂ catalyst at room temperature. The datum is listed on entry 10 in Table 1. Open and red-closed circles indicate the conversion of 2-cyclohexen-1-one and the yield of the corresponding silyl enol ether, respectively. Ni: 4 mol%; *i.e.*, the number of surface Ni atoms of Ni₃Ga/SiO₂ (250 mg, Ni: 5 wt%) is 4% of the mole of 1-cyclohexen-1-one of the substrate, which is explained in the comment on Figure S11.

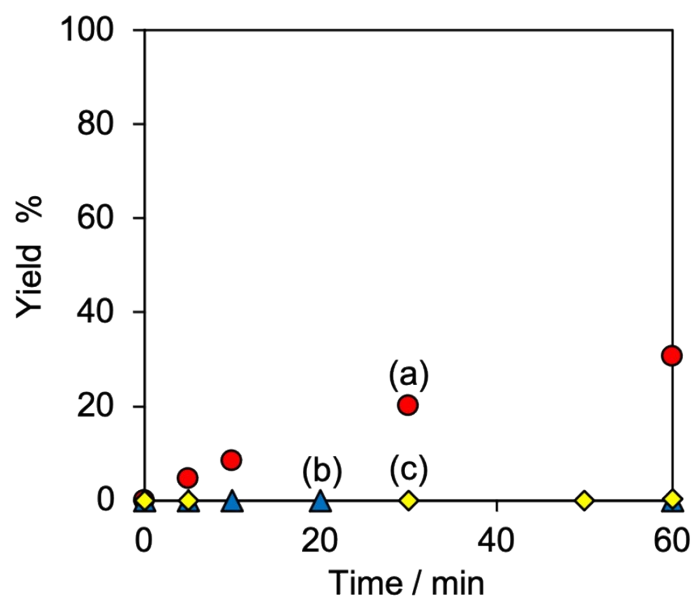


Figure S4. Time course of the hydrosilylation of 2-cyclohexen-1-one over the $\text{Ni}_3\text{Ga}/\text{SiO}_2$ catalyst (a) with pre-treatment (b) without pre-treatment, and (c) Ga/SiO_2 . The symbols indicate the yields of the corresponding silyl enol ether. Catalysts: 250 mg, zeolite: 250 mg, THF: 5 mL, triethylsilane: 0.2 mmol, 2-cyclohexen-1-one: 0.1 mmol, dodecane: 0.1 mmol, under Ar (1 bar), room temperature. The Ga/SiO_2 was prepared by the same protocol as that of the optimum $\text{Ni}_3\text{Ga}/\text{SiO}_2$ catalyst and the amount of Ga loaded was the same as that of constituent Ga component of $\text{Ni}_3\text{Ga}/\text{SiO}_2$ (Ni: 5wt%). Ni: 4 mol%; *i.e.*, the number of surface Ni atoms of $\text{Ni}_3\text{Ga}/\text{SiO}_2$ (250 mg, Ni: 5 wt%) is 4% of the mole of 1-cyclohexen-1-one of the substrate, which is explained in the comment on Figure S11.

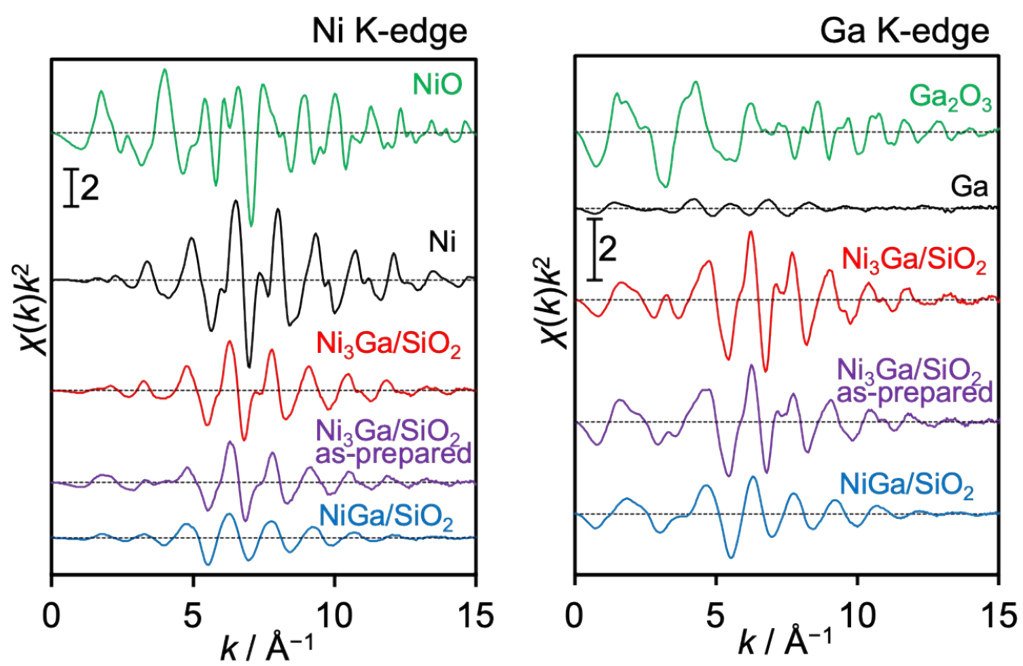


Figure S5. EXAFS oscillations of $\text{Ni}_3\text{Ga}/\text{SiO}_2$, as-prepared $\text{Ni}_3\text{Ga}/\text{SiO}_2$, NiGa/SiO_2 , NiO , Ga_2O_3 , Ni , and Ga .

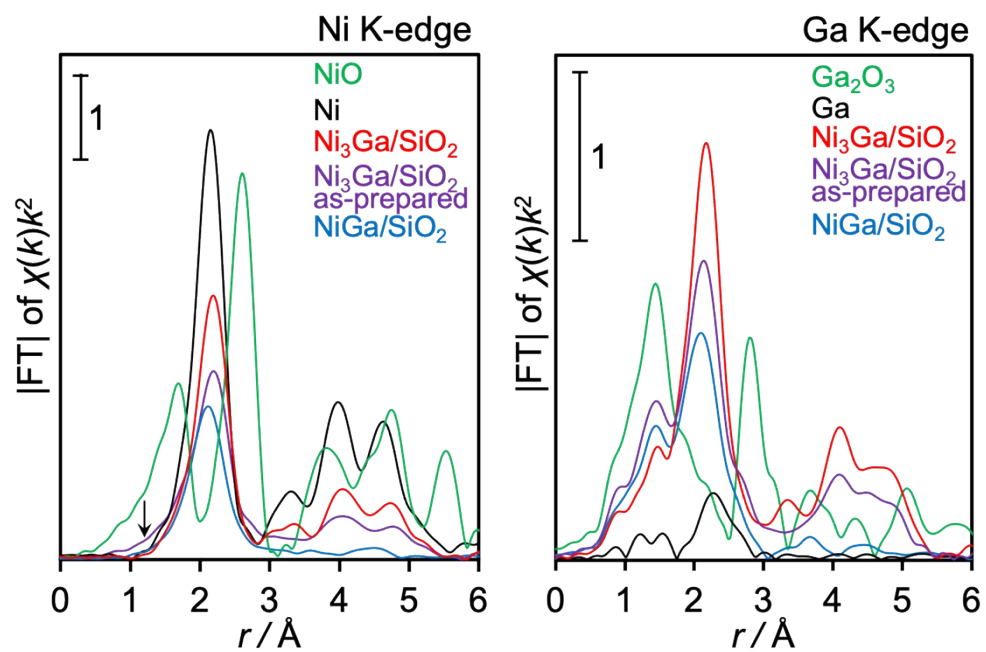


Figure S6. Fourier transforms of EXAFS oscillations of Ni₃Ga/SiO₂, as-prepared Ni₃Ga/SiO₂, NiGa/SiO₂, NiO, Ga₂O₃, Ni, and Ga.

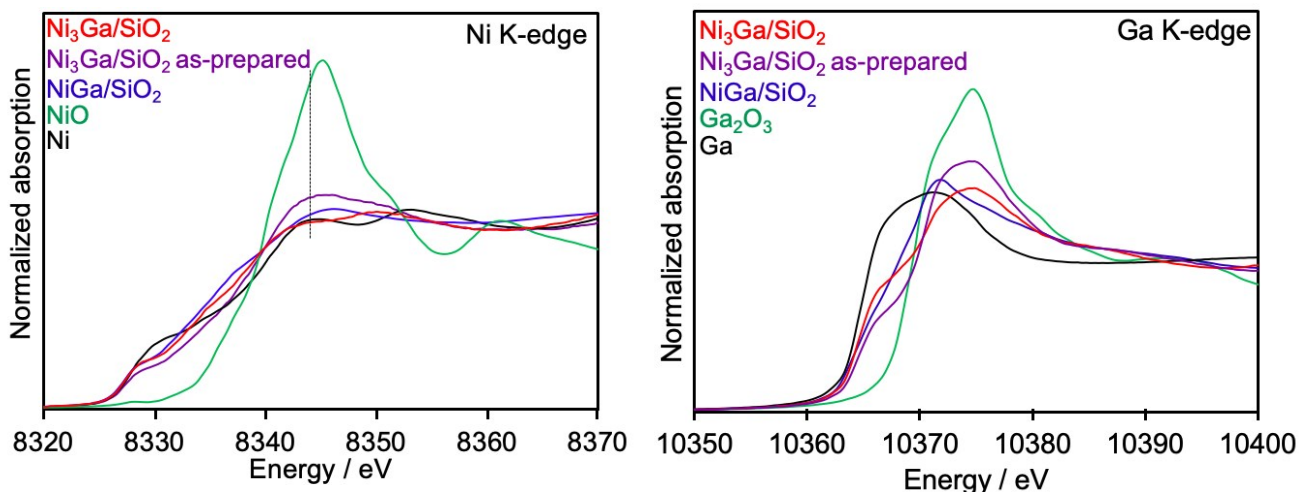


Figure S7. XANES spectra of $\text{Ni}_3\text{Ga}/\text{SiO}_2$, as-prepared $\text{Ni}_3\text{Ga}/\text{SiO}_2$, NiGa/SiO_2 , NiO , Ga_2O_3 , Ni , and Ga .

Comment on the XAFS analyses shown in Figures S5–S7:

X-ray absorption fine structure (XAFS) of $\text{Ni}_3\text{Ga}/\text{SiO}_2$ was recorded so as to discuss the structural and electronic states. Extended X-ray absorption fine structure (EXAFS) is the powerful tool to clarify the local structure in the neighborhood of X-ray-absorbed atoms, which avails to identify the formation of intermetallic compound Ni_3Ga phase. Ni K-edge and Ga K-edge EXAFS oscillations of $\text{Ni}_3\text{Ga}/\text{SiO}_2$ and reference samples are summarized in Figure S5. $\text{Ni}_3\text{Ga}/\text{SiO}_2$ gave similar oscillation to that of Ni foil, suggesting that the Ni atoms in $\text{Ni}_3\text{Ga}/\text{SiO}_2$ is located in surrounding similar to that of monometallic Ni which possesses the face-centered cubic (fcc)-type structure (Fmm). This is consistent with the space group of Ni_3Ga (Pmm). The Ni K-edge EXAFS oscillation of as-prepared $\text{Ni}_3\text{Ga}/\text{SiO}_2$ was almost similar to that of $\text{Ni}_3\text{Ga}/\text{SiO}_2$, while there was a little difference from that of $\text{Ni}_3\text{Ga}/\text{SiO}_2$ in the range below 5 of the k values. For NiGa/SiO_2 , its Ni K-edge EXAFS oscillation disagreed with that of $\text{Ni}_3\text{Ga}/\text{SiO}_2$. This indicates that the local structure in the neighborhood of X-ray-absorbed Ni atoms in NiGa/SiO_2 differs from those in $\text{Ni}_3\text{Ga}/\text{SiO}_2$. For the Ga K-edge EXAFS, the oscillations of $\text{Ni}_3\text{Ga}/\text{SiO}_2$, as-prepared $\text{Ni}_3\text{Ga}/\text{SiO}_2$, and NiGa/SiO_2 were dissimilar to that of monometallic Ga . This would be related to alloying of Ga with Ni .

Fourier transforms of Ni K-edge and Ga K-edge EXAFS oscillations of $\text{Ni}_3\text{Ga}/\text{SiO}_2$ and the reference samples are shown in Figure S6. For the Ni-K edge, $\text{Ni}_3\text{Ga}/\text{SiO}_2$ and NiGa/SiO_2 did not show determinate peak assigned to NiO , whereas as-prepared $\text{Ni}_3\text{Ga}/\text{SiO}_2$ gave slight shoulders which could be related to formation of NiO (as described in the arrow symbol). In contrast, for the Ga K-edge, all the supported Ni-based intermetallic compounds exhibited certainly the peaks located at the position at which the maximum peak of Ga_2O_3 was observed, suggesting the existence of oxidized gallium in all the Ni-based ones.

Ni K-edge and Ga K-edge X-ray absorption near edge structures (XANES) of $\text{Ni}_3\text{Ga}/\text{SiO}_2$ and reference samples are summarized in Figure S7. For the Ni K-edge XANES spectra, $\text{Ni}_3\text{Ga}/\text{SiO}_2$ gave

the different structure of the pre-edge shoulder from that of Ni foil. This would be attributed to hybridization of *p* and *d* orbitals of Ni by alloying with Ga as reported in the XANES analysis of Ni₃Ga bulk.² Moreover, the absorption intensity of Ni₃Ga/SiO₂ above the main edge (as described in dashed line) was lower than that of Ni foil. These would be attributed to electron transfer from Ga atoms to Ni atoms upon alloying with Ga as discussed in the literature.² NiGa/SiO₂ and as-prepared Ni₃Ga/SiO₂ showed similar pre-edge shoulder structures to that of Ni₃Ga/SiO₂. These are evidence of alloying Ni with Ga. However, the absorption intensities above the main edge of NiGa/SiO₂ and as-prepared Ni₃Ga/SiO₂ were higher than that of Ni foil, suggesting that NiGa/SiO₂ and as-prepared Ni₃Ga/SiO₂ contained nickel oxide phases. For the Ga K-edge XANES spectra, the structures around the threshold of Ni₃Ga/SiO₂, as-prepared Ni₃Ga/SiO₂, and NiGa/SiO₂ clearly differed from that of monometallic Ga, which would be related to formation of the Ni-based intermetallic compound phase.² However, the maximum of the XANES spectrum of as-prepared Ni₃Ga/SiO₂ was higher than that of Ni₃Ga/SiO₂, indicating oxidization of a part of gallium of the as-prepared Ni₃Ga/SiO₂ sample.

The presence of the oxidized gallium species of Ni₃Ga/SiO₂ is most likely attributed to aerobic oxidation of a part of surface gallium by sub-ppm-level contaminated oxygen in the glove box during sample preparation, judging from the H₂-TPR profile (Figure S8) and according to the literatures showing formation of Ni-Co-Ga ternary alloy³ in hydrogen stream at 850°C and the high oxophilic property^{4,5} of the gallium.

Thus, the XAFS analyses confirmed that electron transfer from Ga atoms to Ni atoms constituted electron-rich Ni atoms *via* formation the intermetallic compound Ni₃Ga on silica.

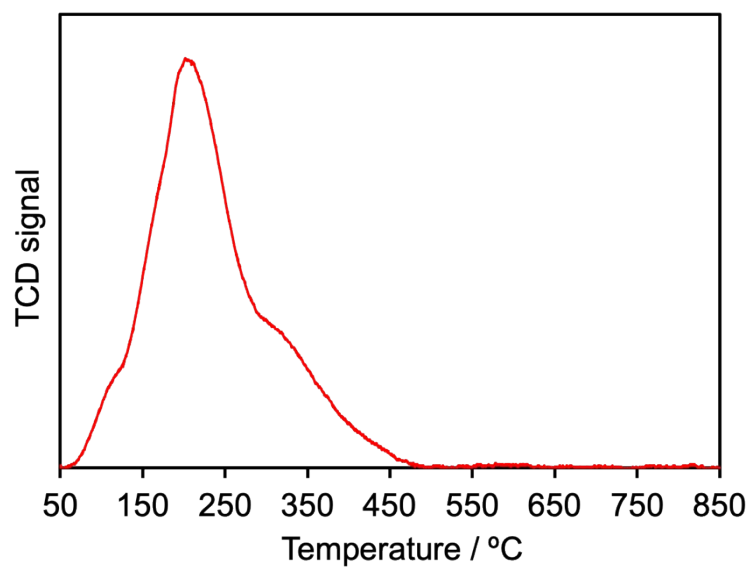


Figure S8. H₂-TPR profile of as-impregnated Ni-Ga/SiO₂ (Ni/Ga = 3) sample.

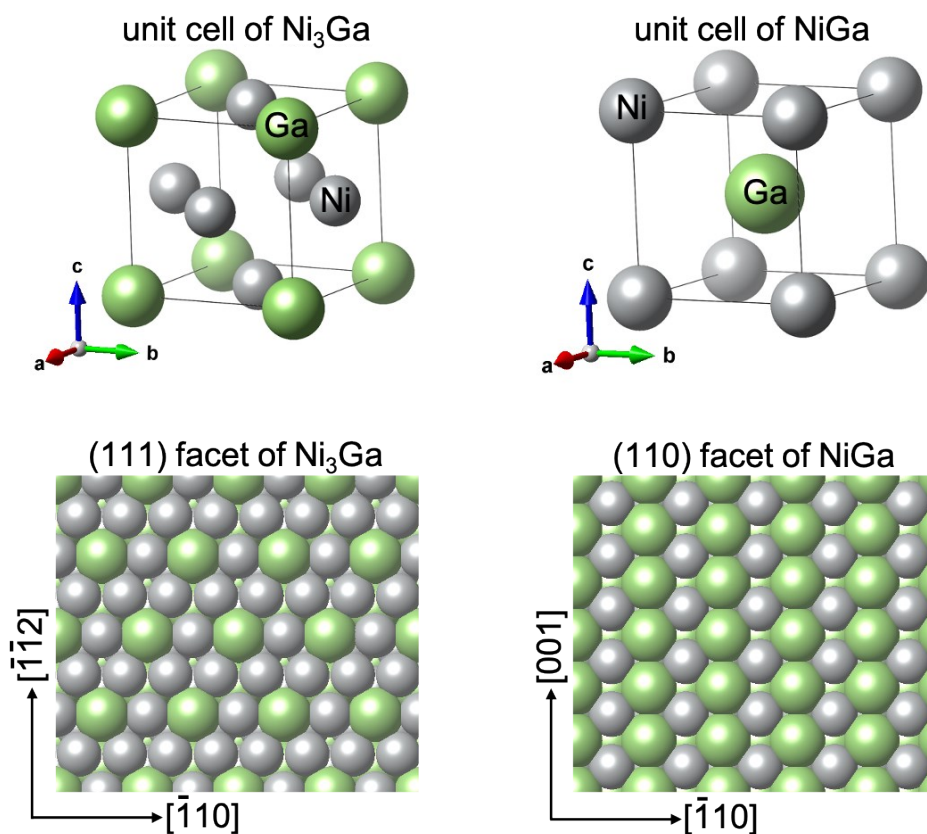


Figure S9. Unit cells of Ni₃Ga and NiGa (upper illustrations) and the representative facets of the thermodynamically stable surfaces of Ni₃Ga and NiGa (lower ones).⁶ These illustrations were drawn using VESTA software.⁷

Comment on Figure S9:

Comparison between the surfaces of Ni₃Ga and NiGa makes differences in their atom arrangements apparent. As for the (111) facet of Ni₃Ga, triangular ensemble sites constructing of three Ni atoms exist, and Ga atoms are isolated upon surrounding with the Ni atoms in this surface. In contrast, in the (110) facet of NiGa, Ga atoms are one-dimensionally aligned with each other neighbor. Accordingly, their Ni atoms are also aligned one-dimensionally without the triangular ensemble sites. As for another different point, the nearest neighbor distance of Ni-Ni atoms in the (110) surface of NiGa (2.89 Å) is longer than that of the (111) surface of Ni₃Ga (2.53 Å). These differences are likely to be one of the key factors to govern catalytic properties of Ni+Ga intermetallic compounds in terms of surface chemistry.

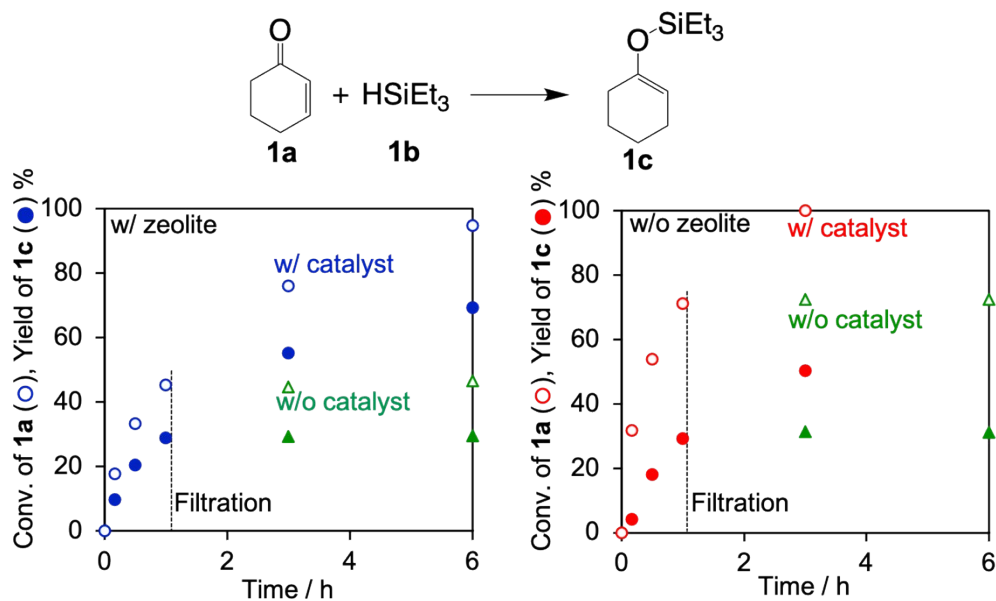


Figure S10. Filtration tests of hydro-silylation over the optimum Ni₃Ga/SiO₂ catalyst under Ar (1 bar) at room temperature. THF: 5 mL, triethylsilane: 0.2 mmol, 2-cyclohexen-1-one: 0.1 mmol, dodecane: 0.1 mmol, catalyst: 250 mg, zeolite: 250 mg. Open and closed triangles indicate the conversion and the yield without catalyst (after filtration of the catalyst and zeolite powders), respectively. Ni: 4 mol%; *i.e.*, the number of surface Ni atoms of Ni₃Ga/SiO₂ (250 mg, Ni: 5 wt%) is 4% of the mole of 1-cyclohexen-1-one of the substrate, which is explained in the comment on Figure S11.

Comment on Figure S10:

Removal of catalyst powder from the reaction solution and analysis of metals contained in the supernatant liquid were performed to exclude the possibility that metals leached from Ni₃Ga/SiO₂ worked as homogeneous catalysts for hydro-silylation. This is evidence that Ni₃Ga/SiO₂ was a heterogeneous catalyst.

As for the left figure, reaction of the hydro-silylation of 2-cyclohexen-1-one was completely stopped upon removing catalyst and zeolite powders at 1 hour of the reaction time (see a difference between blue and green plots after the filtration). The supernatant liquid at 6 hours of the reaction time (blue plots; w/ catalyst) was extracted and analyzed by inductively coupled plasma optical emission spectroscopy (ICP-OES), in which no Ni and Ga species were detected. As for the right figure, removal of catalyst powder gave the same outcome as those in the left one even without zeolite powder as well as no detection of Ni and Ga species by ICP-OES, which is attributed to no elution of the Ni and Ga metals rather than adsorption of the eluted metals on zeolite. These strongly suggest that Ni₃Ga/SiO₂ is a heterogeneous catalyst for the hydro-silylation of 2-cyclohexen-1-one.

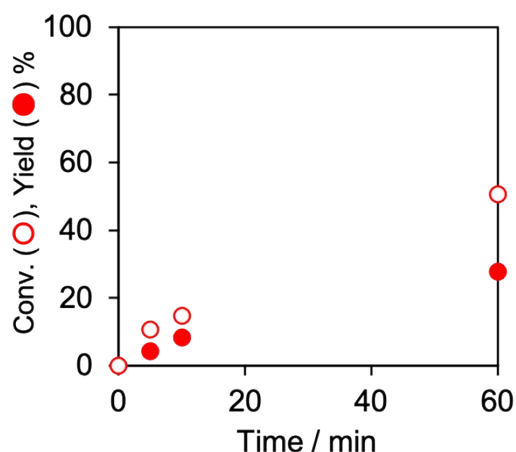


Figure S11. Time course of the hydrosilylation of 2-cyclohexen-1-one over the Ni₃Ga/SiO₂ catalyst at room temperature. Open and red-closed circles indicate the conversion of 2-cyclohexen-1-one and the yield of the corresponding silyl enol ether, respectively. Catalyst: 250 mg, zeolite: 250 mg, THF: 5 mL, triethylsilane: 0.2 mmol, 2-cyclohexen-1-one: 0.1 mmol, dodecane: 0.1 mmol, under Ar (1 bar). The Ni₃Ga catalyst was prepared by the optimized procedure.

Comment on the Figure S11:

The value of TOF (turnover frequency on the Ni atoms of the Ni₃Ga/SiO₂ catalyst surface) for hydrosilylation was estimated by the following equation;

$$\text{TOF h}^{-1} \text{ (per surface Ni atom)} = \frac{\frac{\text{Yield}(\% \text{ at } 1\text{h})}{100} \times \text{mole of the substrate (mol)} \times N_A}{\text{mole of the Ni loaded (mol)} \times \frac{\text{Ni metal dispersion}(\%)}{100} \times N_A}$$

where, N_A indicates the Avogadro constant. The yield of the silyl enol ether was recorded at 1 h of the reaction time. The Ni metal dispersion of the Ni₃Ga/SiO₂ catalyst was measured to be 1.87% by the chemisorbed CO analysis using BELCAT II (Microtrac BEL).

The number of surface Ni atoms of Ni₃Ga/SiO₂ (250 mg, Ni: 5 wt%) corresponds to approximately 4% of the mole of substrate (0.1 mmol), such as 2-cyclohexen-1-one. This is because the total amount (5 wt%) of Ni loaded of the Ni₃Ga/SiO₂ catalyst corresponds to 210% of the mole of the substrate. Accordingly, the number of the surface Ni atoms is mostly described as “4 mol%” in Figures and Tables.

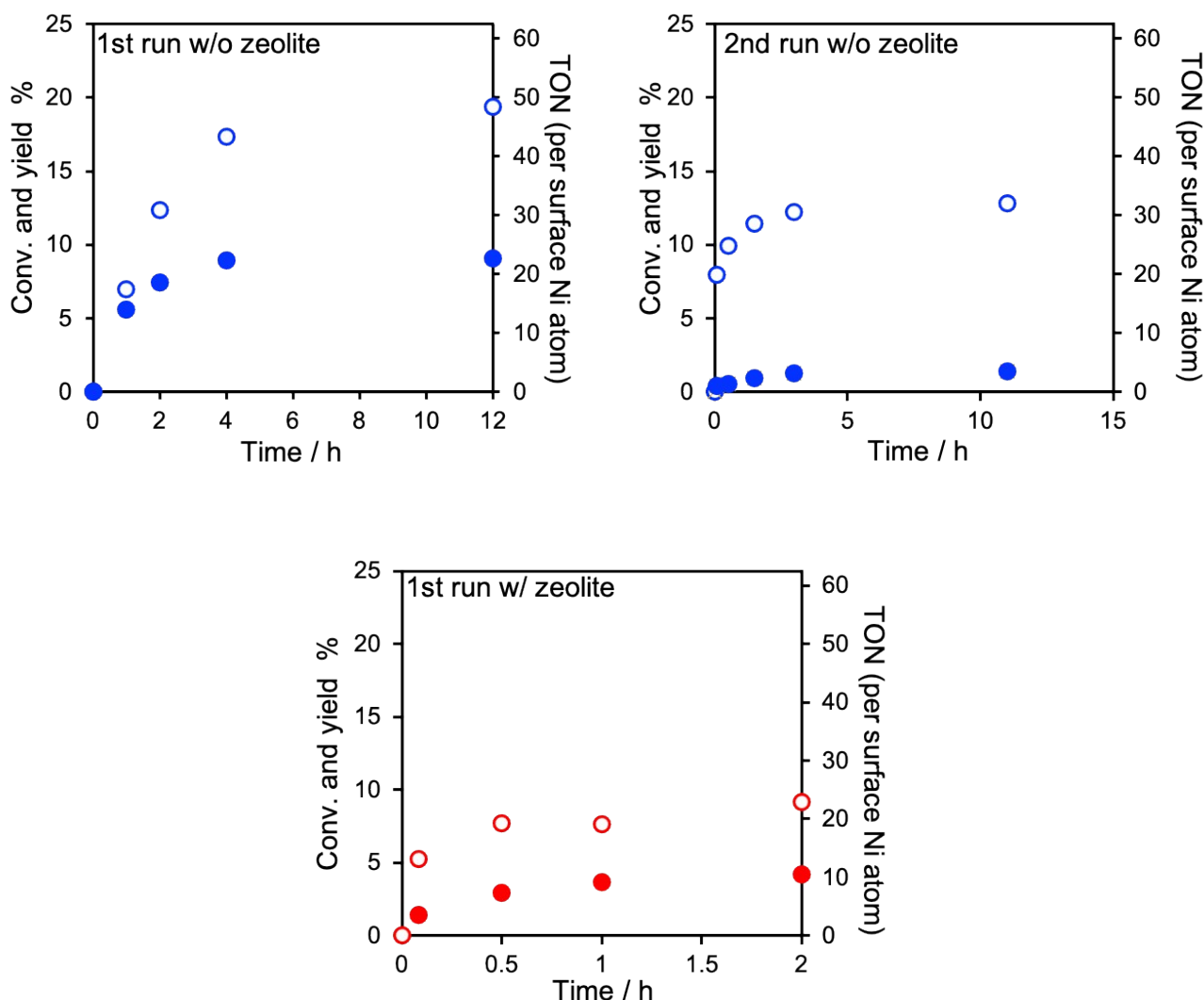


Figure S12. Recyclability of $\text{Ni}_3\text{Ga}/\text{SiO}_2$ catalyst with/without zeolite for hydrosilylation of 2-cyclohexen-1-one by triethylsilane at room temperature. Open and closed circles indicate conversion of 2-cyclohexen-1-one and yield of the corresponding silyl enol ether, respectively. THF: 1.6 mL, triethylsilane: 2 mmol, 2-cyclohexen-1-one: 1 mmol, dodecane: 0.1 mmol, catalyst: 250 mg, zeolite: 250 mg, under Ar (1 bar). Right vertical axes display TON values of the reacted 2-cyclohexen-1-one per surface Ni atom. Ni: 0.4 mol%; *i.e.*, the number of surface Ni atoms of $\text{Ni}_3\text{Ga}/\text{SiO}_2$ (250 mg, Ni: 5 wt%) is 0.4% of the mole of 1-cyclohexen-1-one of the substrate, according to the comment on Figure S11.

Recycle procedure: after 1st run, the solution was extracted by a glass syringe equipped with a syringe filter. And then, the post-reaction catalyst was washed with 20 mL of ethanol and decantation of the slurry was carried out. This was repeated three times. After that, residual ethanol was vaporized under dry Ar stream at room temperature for 20 min then at 70°C for 20 min, followed by hydrogen pre-treatment shown in experimental details in ESI.

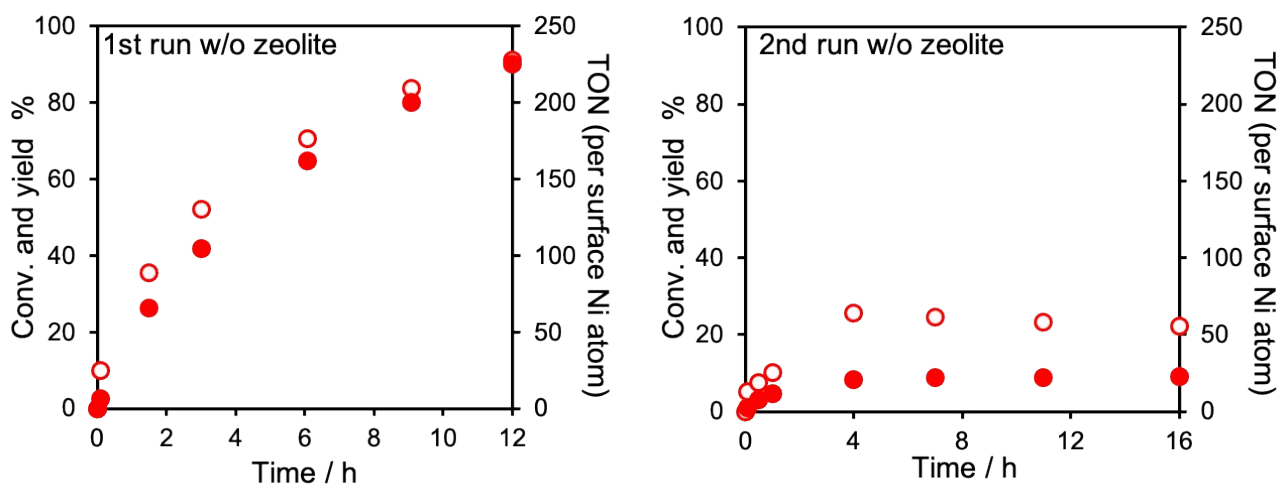


Figure S13. Recyclability of Ni₃Ga/SiO₂ catalyst without zeolite for hydrosilylation of pentanal by triethylsilane at room temperature. Open and closed circles indicate conversion of pentanal and yield of the corresponding silyl ether, respectively. THF: 1.6 mL, triethylsilane: 2 mmol, pentanal: 1 mmol, dodecane: 0.1 mmol, catalyst: 250 mg, under Ar (1 bar). Right vertical axes display TON values of the reacted pentanal per surface Ni atom. Recycle procedure was the same manner as Figure S12. Ni: 0.4 mol%; *i.e.*, the number of surface Ni atoms of Ni₃Ga/SiO₂ (250 mg, Ni: 5 wt%) is 0.4% of the mole of pentanal of the substrate, according to the comment on Figure S11.

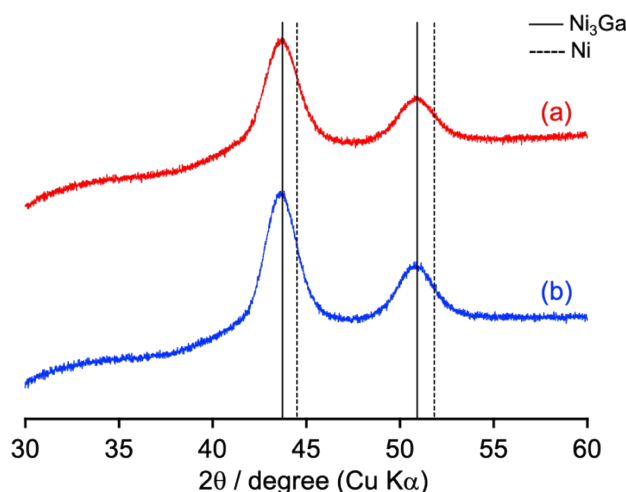


Figure S14. XRD patterns of (a) fresh and (b) spent $\text{Ni}_3\text{Ga}/\text{SiO}_2$ catalyst for hydrosilylation shown in Figure S12. The accumulation times of the X-ray diffractions were 3 times longer than those shown in Figure S2 owing to $0.1^\circ/\text{min}$ of the scan rates. Solid and broken black lines indicate the diffraction peak positions of Ni_3Ga (PDF: 1-71-8620) and Ni (PDF: 4-850), respectively.

Comment on Figures S12–S14:

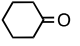
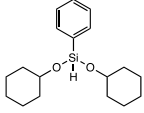
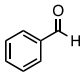
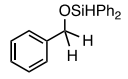
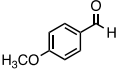
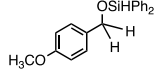
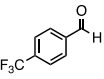
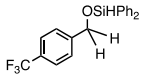
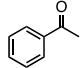
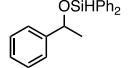
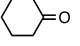
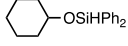
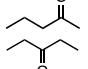
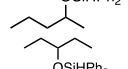
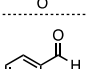
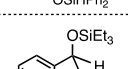
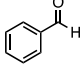
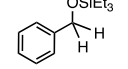
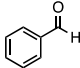
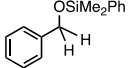
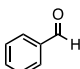
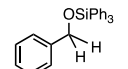
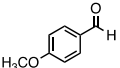
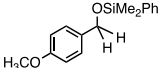
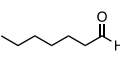
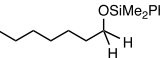
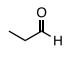
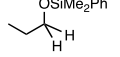
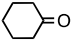
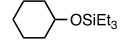
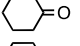
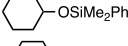
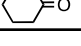
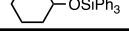
Recyclability of the Ni_3Ga catalyst for the hydrosilylation of 2-cyclohexen-1-one was evaluated (Figure S12). Note that concentrations of 2-cyclohexen-1-one and triethylsilane were 10 times higher than those in Tables 1 and 2 on the main text. Conversion and yield values became almost plateau below 10% (left axis) within 2 hours (see the open and closed red plots; 1st run w/ zeolite). Tendency for these values to become plateau significantly below 100% was similarly observed in the case of no zeolite usage, though maxima of those values approximately twice than those using zeolite (see the open and closed blue plots; 1st run w/o zeolite). Then, recyclability of the post-reaction Ni_3Ga catalyst w/o zeolite was evaluated. However, the values of conversion and yield went down (see the open and closed blue plots; 2nd run w/o zeolite). The reason why their conversion did not reach 100% might be oligomerization of 2-cyclohexen-1-one with reference to the literatures about Pt-based complex catalysts for the hydrosilylation of olefines.⁸ Thermogravimetry and differential thermal analysis (TG-DTA) implied residual ethanol contained in the spent catalyst powder (approximately 2 wt%, data not shown), which might be related to coking *via* the hydrogen pretreatment for the 2nd run considering that coke is often formed on ethanol steam reforming over Ni-based heterogeneous catalysts.⁹ These might be the reason why the recyclability was insufficient in our case.

Next, turnover number (TON) was discussed. XRD patterns of the spent catalyst was recorded as shown in Figure S14 and suggested that the bulk structure and crystallite size were retained after the 2nd run. Considering no elution of constituent metals of Ni_3Ga catalyst into the reaction solution, which is explained in the comment on Figure S10, it is probable that TON is defined as the ratio of the number of reacted 2-cyclohexen-1-one to the number of the Ni atoms of the catalyst surface. In this study, the number of the Ni atoms was estimated by CO-pulse chemisorption measurement (see

experimental details in ESI and the comment on Figure S11). The right vertical axes of the graphs in Figure S12 indicate the TON values. Maximum TON value on the yield was approximately 23 (closed blue plot, 1st run w/o zeolite). We further evaluated the TON value and recyclability in the hydrosilylation of pentanal, which gave the corresponding silyl ether in high yield as shown in Table 2 in the main text. As shown in Figure S13, maximum TON value on the yield reached about 230, though the TON values became almost plateau in 2nd run similarly to that in Figure S12.

Thus, although the recyclability was insufficient at the present stage, these indicated that hydrosilylation over $\text{Ni}_3\text{Ga}/\text{SiO}_2$ proceeded catalytically.

Table S2. Summary of the catalytic performances of the Ni-based complexes and nanoparticles for hydrosilylation.

Entry	Catalyst	Time / h	Temp. / °C	Substrate	Silane	Product	Conv. %	Yield %	TON	Ref. No.
1	Ni 1	24	25		H ₃ SiPh		93	88	18	10
2	Ni 2	5.9	r.t.		H ₂ SiPh ₂		>98	99	20	11
3	Ni 2	2.7	r.t.		H ₂ SiPh ₂		>98	98	20	11
4	Ni 2	110	r.t.		H ₂ SiPh ₂		>98	92	18	11
5	Ni 3	12	r.t.		H ₂ SiPh ₂		100	94	47	12
6	Ni 3	3	r.t.		H ₂ SiPh ₂		100	89	45	12
7	Ni 3	24	60		H ₂ SiPh ₂		100	83	42	12
8	Ni 3	36	60		H ₂ SiPh ₂		100	76	38	12
9	Ni/C	5	120		HSiEt ₃		100	81	1350	13
10	Ni/C	5	120		HSiMe ₂ Ph		100	99	1650	13
11	Ni/C	5	120		HSiPh ₃		100	0	0	13
12	Ni/C	48	120		HSiMe ₂ Ph		95	72	1200	13
13	Ni/C	24	120		HSiMe ₂ Ph		100	70	1167	13
14	Ni/C	24	120		HSiMe ₂ Ph		98	69	1150	13
15	NiCo	24	90		HSiEt ₃		85	50	4 ^{a)}	14
16	NiCo	24	90		HSiMe ₂ Ph		100	100	7 ^{a)}	14
17	NiCo	24	90		HSiPh ₃		11	0	0 ^{a)}	14

r.t.: room temperature, Me: methyl group, Et: ethyl group, Ph: phenyl group. Regarding the detailed structures of the Ni complexes (Ni **1**, **2**, and **3**), please see the corresponding references. ^{a)} TON values are estimated from the total mole of Ni contained in the NiCo catalyst but not from the number of the surface Ni atoms. The mole of impregnated Ni is the same as that of impregnated Co.

Comment on Table S2:

Comparison of reaction temperatures and TON values for hydrosilylation of carbonyls using Ni-based catalysts, such as complexes and nanoparticles, is helpful to distinguish their superiorities. First, in the context of this, catalytic properties of theirs in the hydrosilylation of cyclohexanone is discussed. The hydrosilylation of cyclohexanone proceeds by using Ni complexes (Ni **1**, Ni **3**) and NiCo bimetallic nanoparticles as the catalysts except when triphenylsilane is used (Table S2, entries 1, 6, 15–17). However, there is a difference in the required reaction temperature. The Ni complexes work as the catalysts at room temperature, though it may be that the NiCo bimetallic catalyst require an elevated reaction temperature, *e.g.*, 90°C. Moreover, the TON values of Ni complexes were 18 and 45, whereas that over NiCo was 7 (Table S2, entries 1, 6 and 16). In our case, the Ni₃Ga catalyst gave approximately 23 of the TON value at room temperature (estimated from entry 4 in Table 2 on the main text). Next, from a standpoint of catalysis for the hydrosilylation of aldehydes, the features of the Ni-based ones are compared. The nanoparticulate Ni catalyst supported on carbon convert various aldehydes, such as benzaldehyde, anisaldehyde, heptanal, and propanal, to the corresponding silyl ethers except when triphenylsilane is used at a somewhat high reaction temperature, *e.g.*, 120°C, though their TON values were ranged from 1150 to 1650 (Table S2, entries 9–14). Meanwhile, Ni complex (Ni **2**) plays a role of a catalyst for the hydrosilylation of various aldehydes at room temperature (Table S2, entries 2–4), resulting in approximately 20 of the TON values. With regard to our Ni₃Ga, this catalyst could accelerate the hydrosilylation of various aldehydes and thereby gave the corresponding silyl ethers in moderate or high yields even at room temperature (see Table 2 on the main text, entries 10–14). Maximum TON value was estimated to be 230 in the hydrosilylation of pentanal as shown in Figure S13. Therefore, although it is necessary to pay attention to a difference in reactivity of hydrosilanes, these show that Ni₃Ga is fairly superior in catalysis for the hydrosilylation of carbonyls at room temperature.

Further comparison between the Ni complexes and the Ni₃Ga catalyst makes feature of the Ni₃Ga catalyst apparent. The Ni₃Ga catalyst accelerated the hydrosilylation of 2- or 3-pentanone even at room temperature (see Table 2 on the main text, entries 6 and 7), though Ni complex (Ni **3**) may require an elevated reaction temperature, *e.g.*, 60°C (Table S2, entries 7 and 8). In contrast, acetophenone is converted to the corresponding silyl ether easily by the Ni complex but not over the Ni₃Ga catalyst (Table S2, entry 5; Table 2 on the main text, entry 9). It is assumed that reactivity of ketones with a bulky moiety is somewhat low over the Ni₃Ga catalyst at the current stage. By directing attention to effects of functional groups such as electron-withdrawing and electron-donating moieties, in hydrosilylation using Ni complex (Ni **2**) as the catalyst, trifluoromethyl group with electron-withdrawing makes a period of time to achieve almost 100% conversion of aldehyde longer, though methoxy group with electron-donating results in a shorter period of the time (Table S2, entries 2–4). Interestingly, the tendency for the period over the Ni₃Ga catalyst is opposite (see Table 2 on the main text, entries 12–14). This implies a different mechanism in hydrosilylation over the Ni₃Ga catalyst from that of the Ni complex in items of the Hammett equation.

These comparisons define the nanoparticulate Ni₃Ga catalyst against the field of the catalysis in the hydrosilylation of carbonyls; *e.g.*, the efficient catalysis for the hydrosilylation of carbonyls at room temperature, and the function of the active sites being different from Ni complex homogeneous catalysts.

References in the supporting information

- 1 B. Ravel and M. Newville, *J. Synchrotron Rad.*, 2005, **12**, 537–541.
- 2 W. F. Pong, K. P. Lin, Y. K. Chang, M.-H. Tsai, H. H. Hsieh, J. Y. Pieh, P. K. Tseng, J. F. Lee and L. S. Hsu, *J. Synchrotron Rad.*, 1999, **6**, 731–733.
- 3 C. Wang, A. A. Levin, S. Fabbri, L. Nasi, J. Karel, J. Qian, C. E. V. Barbosa, S. Ouardi, F. Albertini, W. Schnelle, H. Borrmann, G. H. Fecher and C. Felser, *J. Mater. Chem. C*, 2016, **4**, 7241–7252.
- 4 G. Wowsnick, D. Teschner, I. Kasatkin, F. Girgsdies, M. Armbrüster, A. Zhang, Y. Grin, R. Schlögl and M. Behrens, *J. Catal.*, 2014, **309**, 209–220.
- 5 G. Wowsnick, D. Teschner, M. Armbrüster, I. Kasatkin, F. Girgsdies, Y. Grin, R. Schlögl and M. Behrens, *J. Catal.*, 2014, **309**, 221–230.
- 6 (a) Y. Xu, M. Yamazaki and P. Villars, *Jpn. J. Appl. Phys.*, 2011, **50**, 11RH02; (b) R. Guérin and A. Guivarc’h, *J. Appl. Phys.*, 1989, **66**, 2122–2128.
- 7 K. Momma and F. Izumi, *J. Appl. Crystallogr.*, 2011, **44**, 1272–1276.
- 8 Y. Nakajima and S. Shimada, *RSC Adv.*, 2015, **5**, 20603–20616.
- 9 J. Vicente, J. Ereña, C. Montero, M. J. Azkoiti, J. Bilbao and A. G. Gayubo, *Int. J. Hydrogen Energ.* 2014, **39**, 18820–18843.
- 10 T. M. Porter, G. B. Hall, T. L. Groya and R. J. Trovitch, *Dalton Trans.*, 2013, **42**, 14689–14692.
- 11 S. N. MacMillan, W. H. Harman and J. C. Peter, *Chem. Sci.*, 2014, **5**, 590–597.
- 12 H. Tafazolian, R. Yoxheimer, R. S. Thakuri and J. A. R. Schmidt, *Dalton Trans.*, 2017, **46**, 5431–5440.
- 13 J. F. Blandeza, I. E.-Adella, A. Primoa, M. Alvaroa and H. García, *J. Mol. Catal. A: Chem.*, 2016, **412**, 13–19.
- 14 N. R. Bennedsen, S. Kramer, J. J. Mielby and S. Kegnæs, *Catal. Sci. Technol.*, 2018, **8**, 2434–2440.